ADVANCED ENERGY MATERIALS

Supporting Information

for *Adv. Energy Mater.,* DOI: 10.1002/aenm.201800466

High-Temperature Atomic Mixing toward Well-Dispersed Bimetallic Electrocatalysts

Fengjuan Chen, Yonggang Yao, Anmin Nie, Shaomao Xu, Jiaqi Dai, Emily Hitz, Yiju Li, Aijiang Lu, Zhennan Huang, Tangyuan Li, Reza Shahbazian-Yassar, and Liangbing Hu**

SUPPLEMENTARY INFORMATION

High Temperature Atomic Mixing Toward Well-Dispersed Bimetallic Electrocatalysts

Fengjuan Chen[1,(a)], Yonggang Yao[1,(a)], Anmin Nie[2,(a)], Shaomao Xu[1], Yiju Li[1], Jiaqi Dai[1], Emily Hitz, Aijiang Lu[1], Zhennan Huang[2], Tangyuan Li[1], Reza Shahbazian-Yassar[2,]* Liangbing Hu[1, *]

[1]Department of Materials Science and Engineering, University of Maryland College Park, College Park, Maryland, 20742

[2]Department of Mechanical and Industrial Engineering, University of Illinois at Chicago, Chicago, IL 60607

(a) Contributed equally

Email: binghu@umd.edu, reza@uic.edu

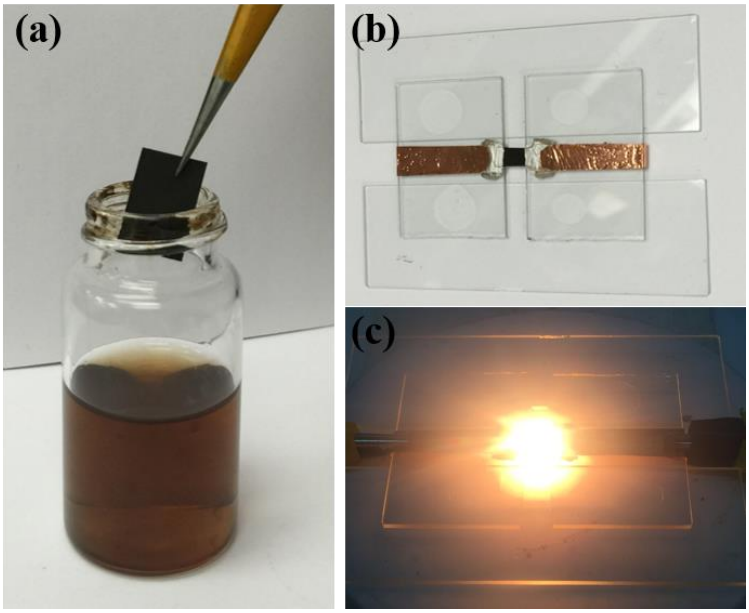

Figure S1. The experimental procedure for the HTP synthesis of bimetallic nanoparticles. (a) The CNF network was soaked in a solution of $PdCl_2$ and $NiCl_2$; (b) the dried CNF network loaded with $PdCl_2$ and $NiCl_2$ was electrically contacted for the Joule heating and cooling process; (c) Joule heating at 1550K was performed on the $PdCl_2$-$NiCl_2$/CNF composite.

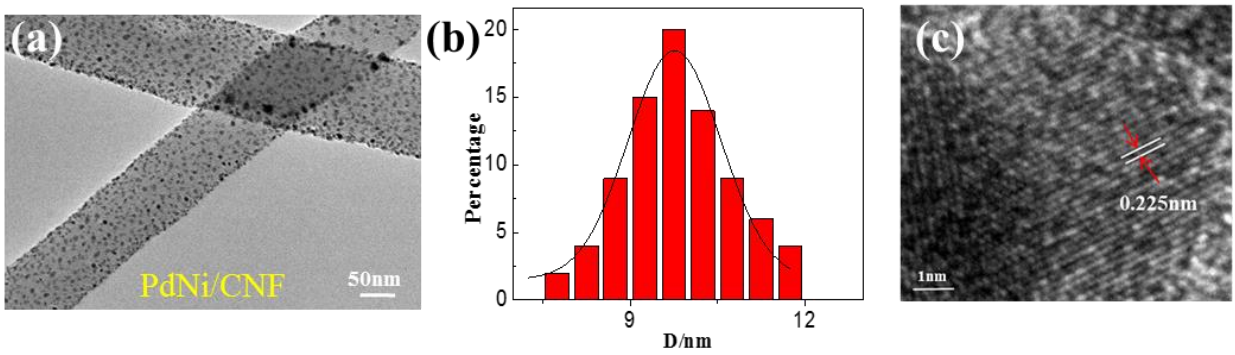

Figure S2. Typical transmission electron microscopy (TEM) characterization of PdNi bimetallic nanoparticles formed on CNF by one-second HTP at 1550K. (a) TEM image of the PdNi nanoparticles on CNF, showing the uniform distribution of particles. (b) The histogram of the size distribution of PdNi nanoparticles showing an average diameter of around 10 nm. (c) HRTEM images of PdNi alloy nanoparticles. The lattice spacing of the fringes is 0.225 nm, corresponding to the (111) plane family.

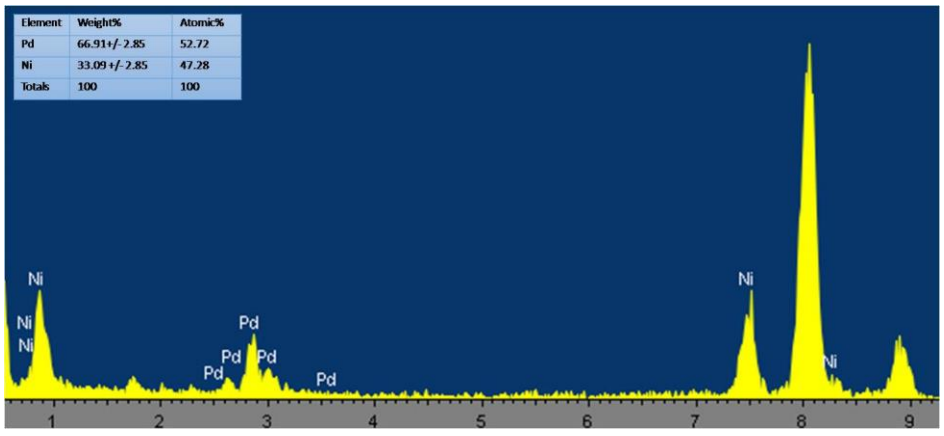

Figure S3. Typical EDX spectrum of Pd and Ni content in the PdNi bimetallic nanoparticles, where peaks correspond to the presence of Pd and Ni. The atomic ratio of Pd/Ni was estimated to be 1.11 Pd to Ni, which agrees well with the molar ratio 1:1 of $PdCl_2$-$NiCl_2$ in the precursor solution.

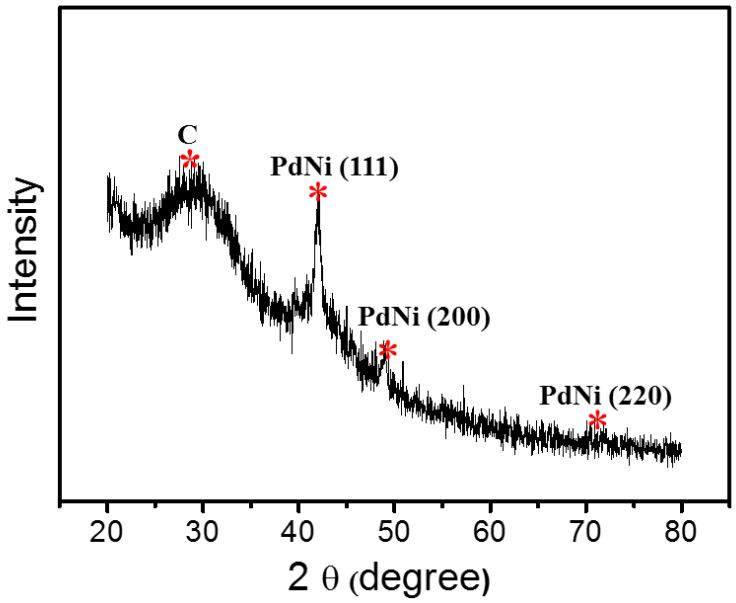

Figure S4. XRD patterns of PdNi alloy nanoparticles on CNF.

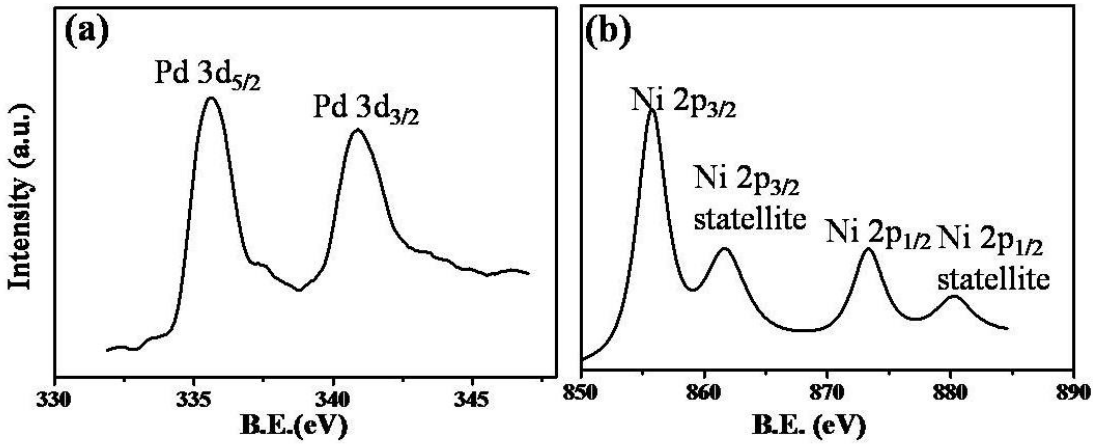

Figure S5. XPS spectra of PdNi nanoparticles on CNF after HTP synthesis. (a) The binding energies of Pd($3d_{5/2}$) and Pd($3d_{3/2}$) for PdNi/CNF. (b) The binding energies of Ni($2p_{3/2}$) and Ni($2p_{1/2}$) for PdNi/CNF. The results show that both signals of Pd(3d) and Ni(2p) shift to higher energy fields compared to that of pure Pd and Ni metal.

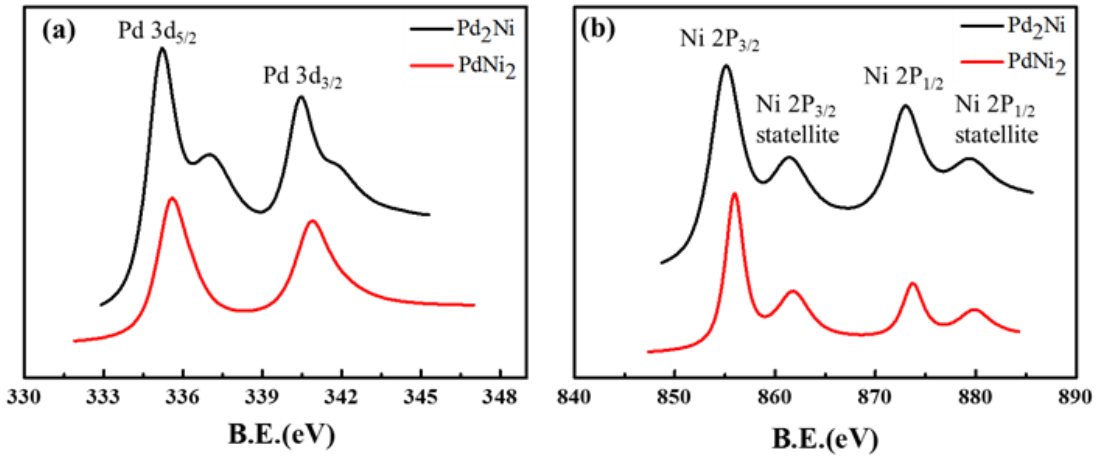

Figure S6. XPS spectra of the Pd 3d and Ni 2p binding energies for $PdNi_2$ and Pd_2Ni. An energy shift to higher energy fields was observed for (a) Pd($3d_{5/2}$) and Pd($3d_{3/2}$) as the Pd molar ratio decreased from 2:1 to 1:2.

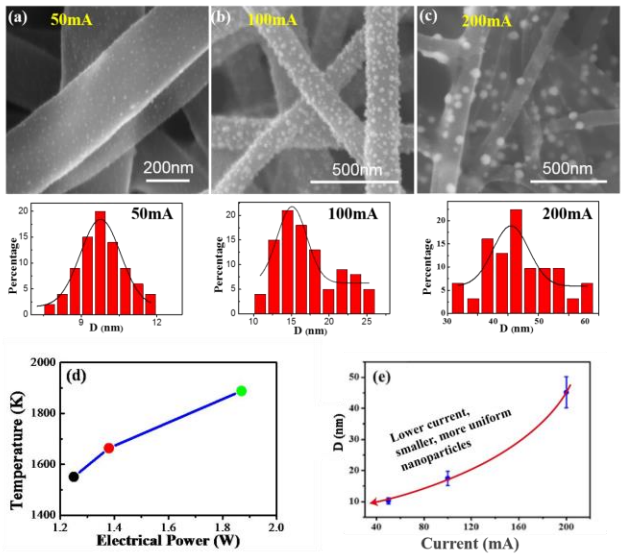

Figure S7. Effect of temperature in HTP process on the size and size distribution of PdNi bimetallic nanoparticles on the CNF network. (a)-(c) SEM images of $PdCl_2$-$NiCl_2$/CNF by 1-second HTP at 50 mA, 100 mA, 200mA, respectively. (d) The temperature of the CNF network under Joule heating using different electrical driving power. (e) Summary of average particle size as a function of Joule heating driven current (temperature). The average particles size increases from 10 ± 1.5 nm to 16.2 ± 2.5 nm to 48.3 ± 5.0 nm with increasing current, confirming the importance of the short pulse for rapid nanoparticle synthesis at a high temperature.

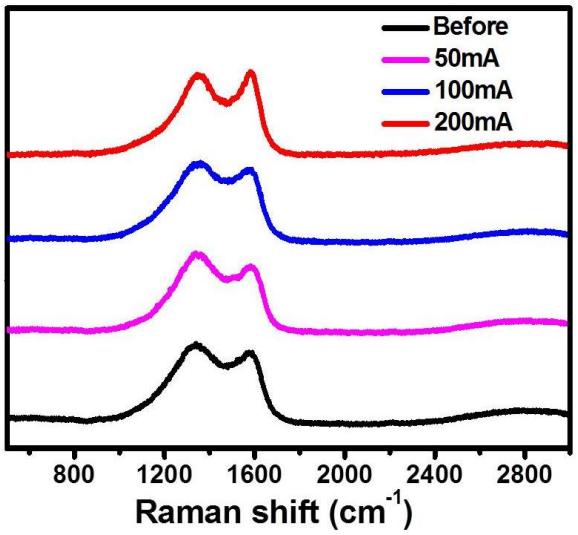

Figure S8. Raman spectroscopy of CNFs before and after HTP treatment at different currents.

Methodology of modeling

In order to study the formation of the Pd core as well as the Ni shell of the nanoparticle, adsorption position and adsorption energy of Ni atoms and Pd atoms on the Pd nanoclusters were calculated via Monte Carlo (MC) simulations. Such calculations were adopted with the module Adsorption Locator included in Materials Studio. The universal force field was selected and the medium quality ensured the accuracy of our analysis. After the core-shell structure was formed, the further heating and cooling down processes were simulated with the molecular dynamics (MD) method. The Discover module in Materials Studio was used, and the heating or cooling processes were realized through NVT and NVE procedures by turns. The dynamic time was longer than 5 ps to ensure a balance of the whole system.

Electrochemical measurement

The HER polarization curves of $PdNi_2$/CNF, Pd_2Ni/CNF, and commercial 40 wt% Pt/C are shown for comparison. The results indicate PdNi/CNF had better performance than other $PdNi_x$/CNF and bare CNFs, but does not yet outperform the commercial 40 wt% Pt/C. However, it should be noted that the estimated loading of our samples was only 5-6 wt% of PdNi/CNF, which may cause the lower performance.

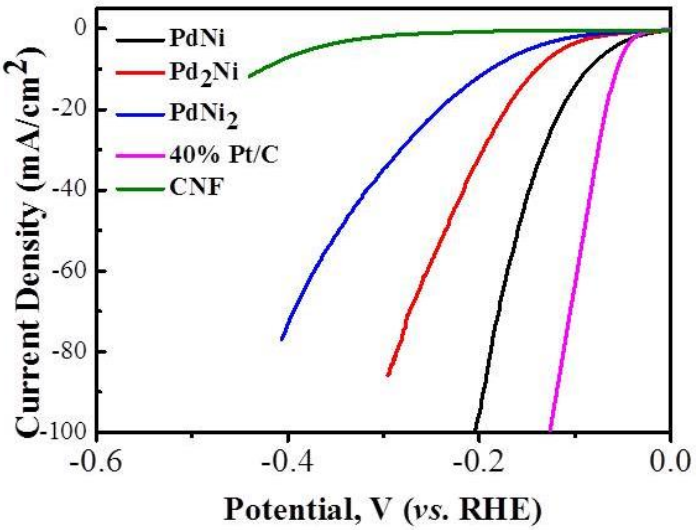

Figure S9. HER polarization curves of PdNi/CNF, Pd_2Ni/CNF, $PdNi_2$/CNF, bare CNF, and 40 wt% Pt/C.

A 1 cm × 1 cm sample was prepared and the HER performance was tested. The larger sample has similar activity compared to the smaller sample.

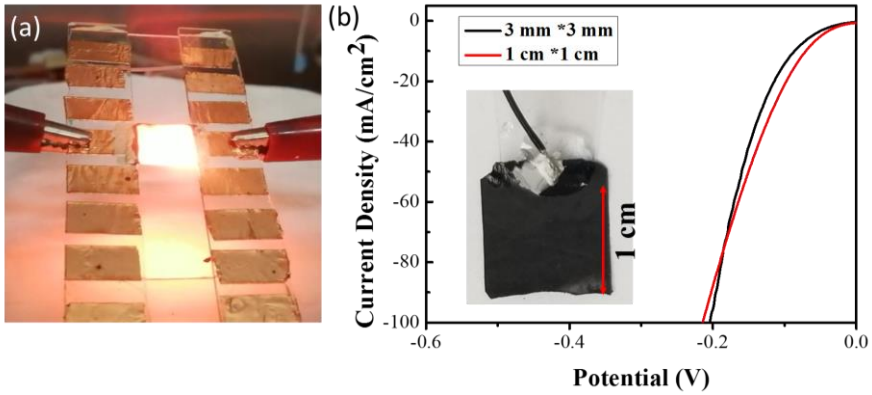

Figure S10. (a) The lighting photo image and (b) HER performance of the 1 cm * 1 cm sized PdNi/CNF sample, demonstrating similar HER performance with smaller sample.

The durability test of HER was performed by applying a constant 150 mV overpotential to the PdNi/CNF sample and monitoring the current density change. After initial stabilization, the current density remained unchanged for over 15 h, indicating the excellent stability of the PdNi/CNF samples at high overpotential.

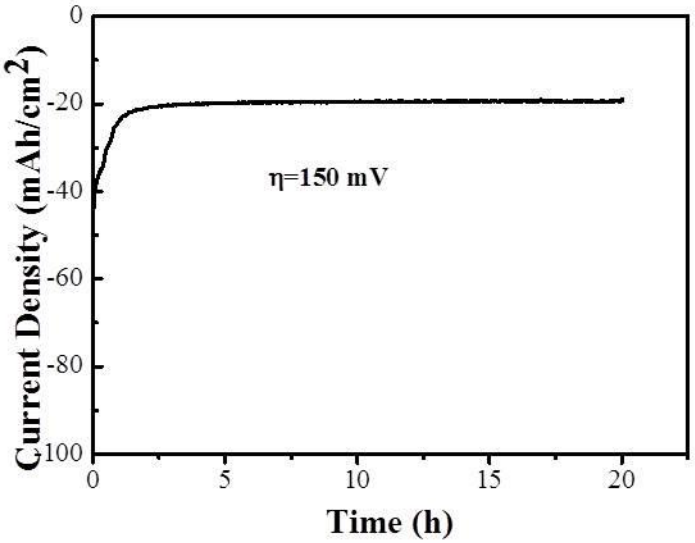

Figure S11. Stability test of PdNi/CNF in acidic solution. The current remained stable over 15 h under a high overpotential of 150 mV.

To clarify the contribution of the oxygen evolution reaction to the H_2O_2 electrooxidation, we tested the performance of the oxygen evolution on the bimetallic PdNi/CNF electrode in oxygen-saturated 4 mol·L^{-1} KOH solution without H_2O_2. As shown in Figure S12, we can observe that the current density of the oxygen evolution reaction is about 0.6 mA·cm^{-2} at 0.2 V, which is much lower than that of the H_2O_2 electrooxidation (281 mA·cm^{-2} at 0.2 V). From these results, we can conclude that the oxygen evolution and carbon oxidation reactions are involved in the H_2O_2 electrooxidation process, but contribute little to the high current density during H_2O_2 electrooxidation.

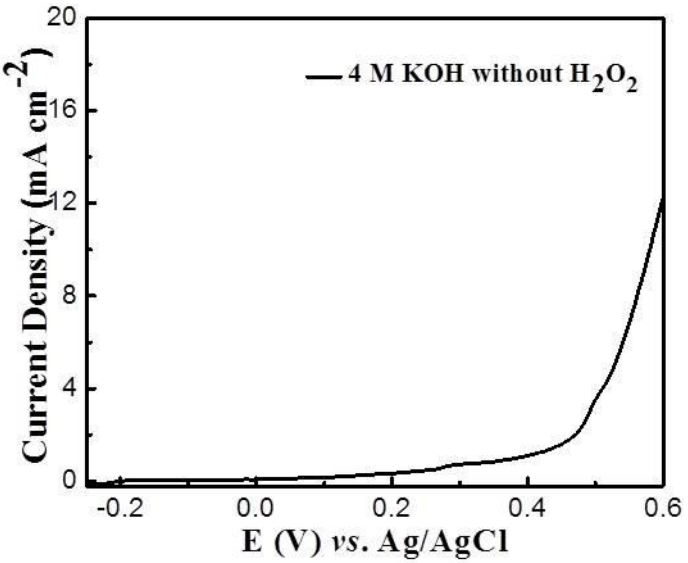

Figure S12. The linear-sweep voltammetry of the PdNi/CNF electrode in 4 mol·L^{-1} KOH without H_2O_2 at a scan rate of 10 mV·s^{-1}.

To demonstrate the generality of this technique, we synthesized bimetallic PtNi nanoparticles on CNFs using the same HTP method. The TEM and associated energy dispersive X-ray spectroscopy (EDS) maps exhibit the uniformly distributed PtNi nanoparticles on the CNF substrate, similar to the PdNi nanoparticles reported in this work.

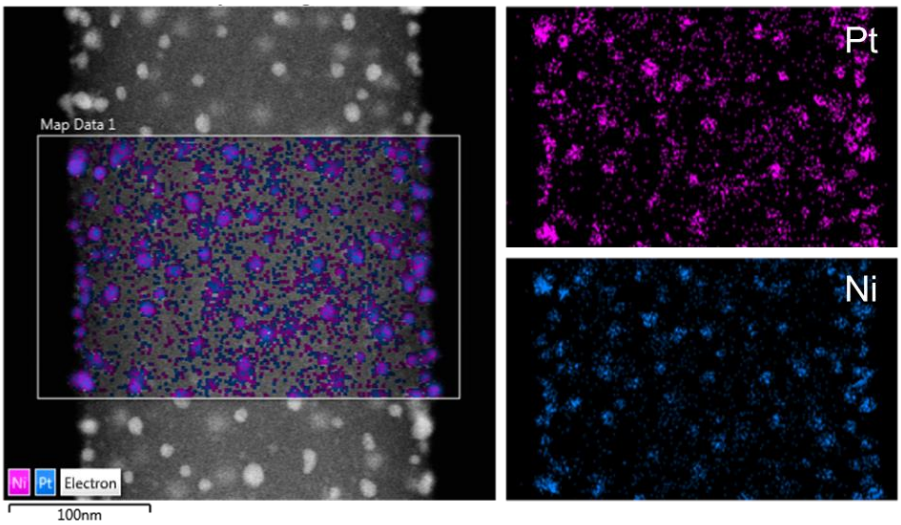

Figure S13. TEM and EDS elemental maps for bimetallic nanoparticles of PtNi/CNF.